Proceedings of ICFDP9:
Ninth International Congress of Fluid Dynamics & Propulsion
December 18-21, 2008, Alexandria, Egypt

ICFDP9-EG-259

INVESTIGATION OF LAMINAR FLOW OVER A BI-WEDGE SHAPE

E. A. A. El-Kady
Associate Prof. Mechanical Engineering Department, Al-Azhar University, Cairo, Egypt
Email : aalkady99@yahoo.com

ABSTRACT

A simultaneous iteration technique to calculate steady laminar, incompressible separation bubbles for two dimensional flow over a bi-wedge is described. The governing equations are written in stream function vorticity formulation. Shear transformation is used to transform the physical domain into a rectangle in the computational domain. Finite difference scheme is applied to descritize the partial differential equations in space. The resulting algebraic difference equations are linearized by Newton method; and Thomas algorithm is employed to solve the block (2 x 2) tri-diagonal matrix using successive line with relaxation (SLR). At each iteration level, the marching solution proceeds from upstream to downstream (boundary layer type solver) until convergence is attained.

Results are presented for $5.66 \times 10^4 \leq Re \leq 5 \times 10^5$, a leading edge apex angle of the bi-wedge of 30°; and a thickness ratio of 0.16. Besides, some numerical results concerning the separated flow over a flat plate with a trough are presented to examine the validity of the present scheme.

Generally, results of the flow over the bi-wedge show that for a given apex angle and thickness ratio as Reynolds number increases the length of separation bubbles increases up to $Re=10^5$ after which the length of the bubble slightly decreases or remains unchanged. Results also show that the bubbles are generally of shallow type.

Key words:

Separation bubble- geometry induced separation- adverse pressure gradient induced separation-successive line with relaxation –upwind differencing

INTRODUCTION

Laminar separation bubbles may occur in a variety of flows in many engineering applications .The flows in turbo-machinary, on the rotor blades of a wind power plants or on hydrofoils are some examples [1-4].Separation bubbles are also found in the field of low Reynolds number aerodynamics such as the case of flows over airfoils with $Re)_{cord}$ up to 10^6 [5]. Separation bubbles are termed as geometry-induced separation or adverse pressure gradient-induced separation depending on the controlling geometrical and operational factors. Along with the occurance of separation on a body is often the formation of irregular motion, eddies ,and even large wakes which sensibly change the flow field structure and boundary layer parameters. Also, associated with the laminar separation bubble is a substational growth of the boundary layer and fluctuations therein, which govern the coefficient of drag of the body. Although the bubble consists of laminar, transition; and turbulent zones [6], it is usually known as laminar separation bubble because the separating boundary layer is laminar [7].The determination and controlling of laminar separation bubbles has been investigated by many investigators, either theoretically or experimentally. Generally, solving through separation bubbles represents a challenge especially for flows which are characterized by large bubbles or flows over bodies where the numerical grid mesh sides in the physical domain is not of orthogonal type (as in the present case). It is seen from survey of the theoretical studies that many models are proposed to predict the separated region as well as the calculation of the boundary layer parameters with a relatively satisfactory

results which compare well with the experimental data [8-10] .The aim of the present study is to calculate the steady two dimensional, laminar separation bubble for incompressible laminar flows around a bi-wedge. The flow around a bi-wedge represents the case where both geometry and adverse pressure gradient-induced separation bubble occur.

A numerical scheme is presented where the finite difference equations of motion are solved by employing successive line with relaxation iterative technique. The results of the flow field variables as well as the important boundary layer parameters are presented for Reynolds number ranging from 5.66×10^4 to 5×10^5.

THEORITICAL ANALYSIS

The problem geometry and the cartesian coordinate system are shown in Fig. (1). The geometry is augmented with three very small circular arcs (radius ≤ 0.02) at points a, b and c to remove singularities at the indicated points; and to force the solution to simulate the physical situation. The wall shape is represented by $y_w(x)$.

The basic equations which describe the motion of steady, laminar, incompressible and two dimensional flows are the Navier-Stokes equations. In cartesian coordinate system the full normalized equations in stream function / vorticity formulation are given as:

$$\psi_{xx} + \psi_{yy} + \omega = 0.0 \qquad (1a)$$

$$u\,\omega_x + v\,\omega_y = 1/Re\,(\omega_{yy} + \omega_{xx}) \qquad (1b)$$

with the usual definition of the vorticity ; velocity and stream function as:

$$\omega = v_x - u_y \qquad (2a)$$

$$u = \psi_y \quad ; \quad \text{and } v = -\psi_x \qquad (2b)$$

The terms neglected in the full equations are higher order and equations (1a) and (1b) are valid for describing many multi-scale phenomena. Equations (1a) and (1b) contain at least all of the ingredients of triple-deck, the first and second order theories provided that the appropriate scales are used.

Following many investigators [11-13], shear transformation is used to transform the physical domain into a rectangle in the computational domain. The new coordinate system (ζ, η) is:

$$\zeta = x \quad , \quad \eta = \frac{y - y_w(x)}{y_e - y_w(x)} \qquad (3)$$

The governing equations (1) in the computational domain are given as:

$$A_1\,\psi_{\eta\eta} + A_2\,\psi_{\zeta\eta} + A_3\,\psi_\eta + \psi_{\zeta\zeta} + \omega = 0.0 \qquad (4a)$$

$$1/H\,(\psi_\eta\,\omega_\zeta - \psi_\zeta\,\omega_\eta) = 1/Re\,(B_1\,\omega_{\eta\eta} + B_2\,\omega_\eta + B_3\,\omega_{\zeta\eta} + \omega_{\zeta\zeta}) \qquad (4b)$$

Where the A's and B's are the scale factor for the stream function and velocity equations respectively. The velocity components u and v are written in terms of ψ as:

$$u = \psi_\eta / H \quad ;$$
$$v = -\psi_\zeta - H`/H\,(\eta - 1)\,\psi_\eta \qquad (5)$$

BOUNDARY CONDITIONS AND DIFFERENCING APPROACH

Due to the symmetry of the geometry about a horizontal plane passing through the leading edge, only one side is used as the solution domain as shown in Fig. (2).The boundary conditions are also shown in that Fig. The appropriate boundary conditions for the upstream $(x = x_i)$ and downstream $(x = x_o)$ boundaries are the same; that is uniform flow assumption is assumed valid. As a result of this assumption:

$\omega = 0.0$; and $\psi_\eta / H(x) = 1$

At the upper boundary (η =1), a streamline is specified in an inviscid flow (ω = 0.0); that is

$\psi(\zeta_i,1) = \psi(\zeta_o,1)$ = constant

At the lower boundary (η = 0.0),

$\omega = 0.0$ and $\psi(\zeta,0)$ = constant = 0.0 $(\zeta < 0.0)$

$\psi = 0.0$ and $\psi_\zeta = 0.0$ $(0.0 \le \zeta \le 1)$
(no slip conditions)

Finite difference approximations (see fig.3) of all derivatives in equations (4) and their boundary conditions results in an algebraic system of coupled equations in the two unknowns ψ and ω. More precisely, central differences are used everywhere except for the convective term ($u\,\omega_\zeta$) which is treated as upwind differencing [14] (backward or forward depending on $u > 0.0$ or $u<0.0$). In the previous work [13], the wall boundary condition ($u = \psi_\eta = 0.0$) is treated as three-point backward difference and the resulting equation is used to generate the recursion constants for the coupled solution. In the present work, the finite difference Poisson's equation is applied at the surface using that wall boundary conditions. The resulting algebraic equation is:

$$2\,\psi(I,2)/(\Delta\eta^2) + \omega(I,1) = 0.0 \qquad (6)$$

Where $\psi(I,2)$ is related to $\omega(I,1)$ [J=1 represents the wall surface] through the recursion relation; so the final equation (6) determines the velocity at the wall. In this way, the wall boundary conditions are applied fully implicitly leading to fast convergence. At each ζ-line in the computational domain, the finite difference equations based on Newton linearization technique have the following general form:

$$a_j\,\psi_{i,j-1} + b_j\,\psi_{i,j} + c_j\,\psi_{i,j+1} + \omega_{i,j} = R_1(j) \qquad (7)$$

$$d_j\,\psi_{i,j-1} + e_j\,\psi_{i,j} + f_j\,\psi_{i,j+1} + E_j\,\omega_{i,j-1} + F_j\,\omega_{i,j} + G_j\,\omega_{i,j+1} = R_2(j) \qquad (8)$$

Equations (7) and (8) are solved iteratively and simultaneously with the successive line and relaxation (SLR) scheme. At each ζ-line, a block (2 x 2) tri-diagonal matrix is solved using Thomas a logarithm. The marching type solution proceeds from upstream inlet plane to downstream exit plane after two or three local iterations at each vertical line to allow for the non-linear terms in the vorticity transport equation. This procedure is applied until one cycle of global iteration is completed. Upon completion, a new cycle is initiated by updating ψ in the computational domain. The global sweeps are repeated until convergence is attained. The convergence criterion is based on maximum allowable difference in ψ obtained from two successive sweeps; namely, maximum $|\Delta\psi| \le 10^{-5}$.

It should be pointed that for all investigated cases the upstream boundary is located at a distance of 8L before the geometry; while the downstream boundary is located at 12 L after the geometry. The upper boundary is located at a vertical distance of at least $y_e = 2L$ which is corresponding to about 11-33 times the thickness ratio. (t/L). The numerical experimentation proved that the results are not influenced by increasing these mentioned values for the location of the boundaries. Also, the computational domain consists of 200x200 (MxN) grid points. The choice of the mesh sizes is determined by the resolution requirements. For example, in the viscous zone in the vicinity of the wall (where large gradients exist) a stretched grid is used to capture the details of the boundary layer. For this purpose, the first mesh size at the wall was chosen as $\Delta\eta = 0.0003$; which a geometric series is employed for growing the mesh sizes at a rate of 1.1. This resulted in about 60 grid points embedded in the boundary layer thickness. In the axial direction, the mesh sizes $\Delta\zeta$ were chosen very small ($\Delta\zeta = 0.005$) at locations of very large axial gradients; namely, around points a, b and c (singular points). Far upstream and far downstream the geometry, coarser mesh sizes of about $\Delta\zeta = 0.2$ were chosen where small gradients exist. Under relaxation was used in the present study. After convergence is attained all flow field properties and boundary layer parameters are calculated.

Wall Coefficient of Friction (C_f)

By definition,

$$C_f = (2\,\tau)/(\rho\, u_\infty^2) \qquad (9)$$

With the given definition of vorticity and after a straight forward substitution, the wall coefficient of friction is given by:

$$C_f = 2\,(\omega + 2\,\omega_\eta / H)_w/(Re) \qquad (10)$$

The term ω_η at wall was evaluated by three-point backward difference.

Wall Coefficient of Pressure (C_p)

To obtain the wall coefficient of pressure, the dimensionless Navier-Stockes equations are applied at the wall in their primitive variables in conjunction with the continuity equation. Upon applying these equations in the (ζ,η) plane and using the definition of the coefficient of pressure and after simple substitution, one obtain:

$$C_p\,(\zeta)|_w = 2/Re\,(H'\,\omega_\zeta + (1+ H'^2 / H)\omega_\eta) \qquad (11)$$

Integration of equation (10) between stations (i-1) and (i) yields:

$$C_p\,(i) = C_p\,(i-1) + 2/Re\,[\,H'\omega\,|_{i-1}^{i} - H''\int_{i-1}^{i}\omega\,d\zeta - \int_{i-1}^{i}(1+H'^2 / H)\omega_\eta\,d\zeta]_w \qquad (12)$$

In equation (12), the term $H'\,\omega_\zeta$ was integrated by parts and the Simpson rule of numerical integration is used to approximate the integrals. The wall coefficient of pressure is considered equal to unity at the stagnation point (a) of the geometry.

Displacement Thickness (δ^*)

With the usual definition of the displacement thickness in two dimensional flow, the non-dimensional displacement thickness in the computational domain is calculated as:

$$\delta^* = H \int_0^{\eta 1} (1 - u)\,d\eta \qquad (13)$$

Where the edge of the boundary layer (η_1) is specified at that distance for which u = 0.995.

RESULTS AND DISCUSSION

The performance of the present numerical scheme has been first evaluated for a two dimensional, incompressible laminar separated flow over a flat plate with a trough. The trough is located downstream of the leading first studied by Carter and Wornom [15] by using the inverse interaction method .Also, many other investigators[12,16] solved the same problem by employing several numerical techniques. The surface of the trough was given by the equation:

$$Y_w(x) = -d.sech\,(4x-10), \quad 0.0 \le x \le 7.5 \qquad (14)$$

Where d is the dimensionless depth of the trough and was set equal to 0.03.The equations are solved in the whole domain by the present technique from upstream boundary to downstream boundary where the elliptic terms $\psi_{\zeta\zeta}$ and $\omega_{\zeta\zeta}$ were set equal to zero at the downstream boundary[12,13].The relaxation factor has been set to 1.2. Fig. 5 (a and b) depicts the present results of the displacement thickness and coefficient of friction respectively compared with those calculated by Halim [12],Carter and Wornom[15] ;and Veldman [16]. As can be seen from Fig.5 an excellent agreement can be noticed between the present results and those of Halim[12] .Halim solved the partially parapolized Navier-Stokes (PPNS) equations in the viscous zone coupled with the inviscid flow equation ; while in the present scheme the Navier-Stokes equations were solved in the whole domain. On the hand the obtained results of the present scheme for the displacement thickness and coefficient of friction are over and under estimated respectively compared with those of references [15] and [16] far upstream and far downstream where good agreement is noticed. In the region of separated flow, the present results are in very good agreement with those of [15] and [16].Carter and Wornom [15] employed an inverse interacting technique; while Veldman[16] employed a quasi-simultaneous method for the boundary layer and

inviscid outer flow equations. The convergence cut-off was considered 10^{-5} in the present work compared to 10^{-4} in the work of [15 and 16].

Fig.(6) presents the distribution of the skin friction coefficient over the bi-wedge for the shown investigated values the dimensionless thickness ratio ,leading edge apex angle; and Reynolds number .The values of C_f in the separation bubble were magnified to be able to see the solution in that region. From this Fig., one can easily notice that there are two peaks of C_f at those locations of very strong viscous and inviscid interaction. These two locations are the leading edge and point b of Fig (1) ; just before separation. Also the obtained numerical results show that the length of the separation bubbles are about 0.15, 0.2276, 0.215; and 0.215 corresponding to Re =56600, 100000,300000; and 500000 respectively. These values of the length of the separation bubbles indicate that increasing Re firstly increases the length of the bubble up to Re=100000; after which the length of the bubble very slightly decreases with Re. This phenomenon of two dimensional separation has been also observed by another investigators [17,18]. Fig.(6b) also shows that the point of separation is somewhat influenced by Re ;and separation takes place earlier with increasing Re. For Re ≥100000 the location of separation takes place at nearly the same position just after point b of Fig.(1) (where x ≈ 0.3). For Re=56600 , separation takes place at a quite small distance downstream of point b.

Fig.(7) representing the results of the wall coefficient of pressure may help in demonstrating the aforementioned results of the separation bubbles over the bi-wedge. Again, the values of C_p in the region of separation were magnified. The important finding which can be obtained from Fig.(7) is that ,the adverse pressure gradient accompanying the flow with Re=56600 is lower than that with the three other investigated values of Re for which the calculated values of the adverse pressure gradient are higher ;in excellent agreement with the work of Youssef [17] and Tani [18] . According to Bernoulli concept this might be expected. These results of the pressure gradient may be the answer about the question why the flow separates more earlier when Re ≥100000 than that when Re=56600 ?.

The development of the axial velocity profiles between the leading and trailing edges is shown in Fig.(8). These profiles are depicted at some selected x-locations for different investigated values of Re. As can be seen from the profiles between the leading edge and point b of Fig.(1) ;where the area of flow is decreased ,the increased convective acceleration of the external stream results in the shown boosting in the profiles and a strong viscid/inviscid interaction occurs. This boosting reaches its maximum at point b (x≈ 0.3) where the area of flow is minimum. According to the continuity principle, this is expected. The velocity gradient in the immediate vicinity of the wall in this region increases in the direction of flow and reaches its maximum at b ; causing the observed increase of C_f as shown in Fig.(6). Downstream x≈ 0.3, the area of flow is increased and the flow rapidly (strongly separated flow) separates from the wall and reattaches again at some distance depending on Re. After reattachment, the external stream decelerates and a boundary layer type flow is noticed in that region until the trailing edge (x=1). Generally, the recirculated velocities in the separation bubbles are relatively very small; and reach their maximum values near the reattachment point around the center of recirculated vortices [6]. Also, the velocity profiles at x = 0.406836 indicate that the separation bubbles are generally of shallow type as the case of flow around symmetric airfoils [12].

Fig.(9) presents the obtained results of the displacement thickness . As can be seen from this Fig., the displacement thickness firstly increases through a very small distance following the leading edge due to the increased viscous layer. After that , the displacement thickness decreases dramatically due to the increased convective acceleration .The minimum values of the displacement thickness are obtained at x≈0.3 ; just before separation corresponding to maximum C_f since under prediction of the displacement thickness corresponds to over prediction of C_f

[12,19] .This is obvious from the velocity profile at this location ;where the viscous layer is seen to be very thin (very strong viscid/ inviscid interaction). After that point , the displacement thickness increases to attain its maximum at the separation point ; where the separating streamline moves away from the surface. After reattachment, the boundary layer behaves like any two dimensional flow; where the boosting in the velocity profiles diminish gradually in the direction of flow; and the growth of the displacement thickness is relatively weak. Besides, Fig.(9) shows that for the same x the displacement thickness decreases as the value of Re increases as the boundary layer thickness inversely proportional to Reynolds number.

CONCLUSIONS

The laminar separation bubbles around a bi-wedge are calculated by solving Navier-Stokes (NS) equations written in stream function/vorticity formulation. The flow field over the trough geometry presented in references (12,15,16) is solved to demonstrate the present scheme. The following statements provide a summary of the most important conclusions:

1.The governing equations are written in a body-aligned coordinate system for two dimensional flow ; and consequently similar flows of practical interest can be solved using the present formulation.

2.The boundary conditions at the surface are described in a fully implicit manner by using central difference representations of the terms of the stream function equation leading to fast convergence.

3.Results of the bi-wedge case showed that the separation bubbles are of shallow type; and the length of the bubble slightly decreases with increasing Re more than Re= 10^5 .

4.The location of the separation point moves slightly upstream as Reynolds number increases.

5.The separation bubbles around the bi-wedge contains slow moving fluid and the center of the recirculated vortices lies near the reattachment point .

REFERENCES

1.Stieger,R.,Hollis,D.,and Hodson, H., "Unsteady surface pressures due to wake induced transition in a laminar separation bubble on LP turbine cascade",proceeding of ASME Turbo-Expo .,June16-19,2003.

2. Brodeur, R. and Van Dam, C.P., "Transition prediction for a two –dimensional Reynolds-averaged N-S method applied to wind turbine airfoils", Journal of wind energy, 2001.

3.Rogers,S.E.,Wiltberger,N.L. Kwak,D.,"Efficient simulation of incompressible viscous flow over single and multi-element airfoils", Journal of aircraft,vol.30,No.5,pp.736-743,1993.

4. Mayda, E.A.,VanDam,C.P.,and,E.P.DuqueN., "Bubble induced unsteadiness on wind turbines airfoils", AIAA, paper-0033,pp.1-12,2002.

5. HA¨ggmark,C.P.,"Investigations of disturbances developing in a laminar separation bubble flow", Technical reports from Royal Institute of Technology,Dept.of MechanicsStockholm,Sweden,2000.

6. Horton,H.P.,"A semi-empirical theory of the growth and bursting of laminar separation bubbles", Aeronautical Research Council ,c.p.1073,1969.

7. Govindarajan ,R.,"A literature survey on laminar separation bubbles ",National Aeronautical laboratory, project Cf 9205,India,1992.

8. Alam,M. and Sandham,N.D.,"Direct numerical simulation of short laminar separation bubbles with reattachment",J.Fluid mechanics 403,pp.223-250,2000.

9.Domenico,D.andRoberto,M.,"Numerical methods for solving three dimensional parabolized Navier-Stockes equations", Institute for numerical applications in science and engineering (ICASE) and NASA Langley Research center No.NASI-19480,1995.

10.HA¨ggmark,C.P,Bakchinov,A.A.,and Alfredsson,P.H.,"Experiments on two dimensional separation bubbles",Phil.Trans.,R.,Soc. London A358,2000.

11.Davis,R.L.and Carter,J.E.,"Three dimensional viscous flow solutions with a vorticity-stream

function formulation", AIAA, vol.27 ,pp.892-900,1989.
12. Halim,A.A.M.,"Global marching technique for predicting separated flows over arbitrary airfoils",AIAA ,vol.25,pp.1263-1266,sep.,1987.
13.El-kady,E.A,"Calculation of separation bubbles around conically-nosed cylinders", proceedings of Al-Azhar University Engineering Third Int. Conference(AEIC), Cairo, Egypt, Desember,1993.
14. Rogers,S.E.and Kwak, D.,"Upwind differencing scheme for the time accurate incompressible Navier -Stockes equations" ,AIAA ,vol.28,No.2,pp.253-262,1990.
15. Carter, J.E. and Wornom, S.F.," Solutions for incompressible separated boundary layers including viscous-inviscid interaction", Aerodynamic analysis requiring advanced computers ,NASA SP-347,pp.125-150,1975.
16.Veldman, A.E.P.," New quasi- simultaneous method to calculate interacting boundary layers '',AIAA,vol.19,No.1,1981.
17. Youssef,F.A. and Said,M.H.," Axisymmetric boundary layer on slender pointed body of revolution",Proceedingsof the 7th.Int.conf.of Mech.Power Engineering, Cairo University,1990.
18. Tani,L.,"Low speed flows involving bubble separation", Prog. Aero.Sci.,5,pp.70-103,1964.
19. Abdalla,I.E. and Yang ,Z. ,"Numerical study of a separated –reattached flow on a blunt plate" ,AIAA Journal, Vol.43, No.12, 2005.

NOMENCLATURE

A1 coefficient appearing in eqn.4a , $(H'^2(\eta-1)^2+1)/H2$
A2 coefficient appearing in eqn.4a , $(2H'(\eta -1))/H$
A3 coefficient appearing in eqn.4a , $(\eta -1)/H^2[2 H'^2 +HH"]$
B1 coefficient appearing in eqn.4b, $(1/H^2)[1+H`^2(\eta-1)^2]$
B2 coefficient appearing in eqn.4b, $(\eta-1)[2H`^2/H^2+H``/H]$
B3 coefficient appearing in eqn.4b, $2*(H`/H)(\eta -1)$
C_f coefficient of friction,$2\tau_{xy}/\rho U_\infty^2$
Cp coefficient of pressure,$2(p-p_\infty)/ \rho U_\infty^2$
H scale factor, $y_e-y_w(x)$
L length of the model
P static pressure
Re Reynolds number. $U_\infty L/\nu$
U_∞ free stream velocity
u dimensionless x-wise velocity, u^*/U_∞
v dimensionless y-velocity component, v^*/U_∞
x dimensionless axial coordinate, x*/L
y dimensionless normal coordinate, y*/L
e upper edge of the solution domain

Greek symbols

α leading edge semi-apex angle
β trailing edge semi-apex angle
δ boundary layer thickness
δ* dimensionless displacement thickness, $\int_0^\delta (1- u)d\eta$
η sheared coordinate in the normal direction
ζ sheared coordinate in the axial direction
ν kinematic viscosity
ρ density of fluid
τ_w wall shear stress in the x-y plane
ω dimensionless vorticity, $\omega^*/U_\infty L$

Subscripts

η,ζ,x,y partial derivative with respect to the indicated variable
w wall conditions
∞ conditions in the free stream

Superscripts

'," primes denote to first and second derivatives with respect to wall shape

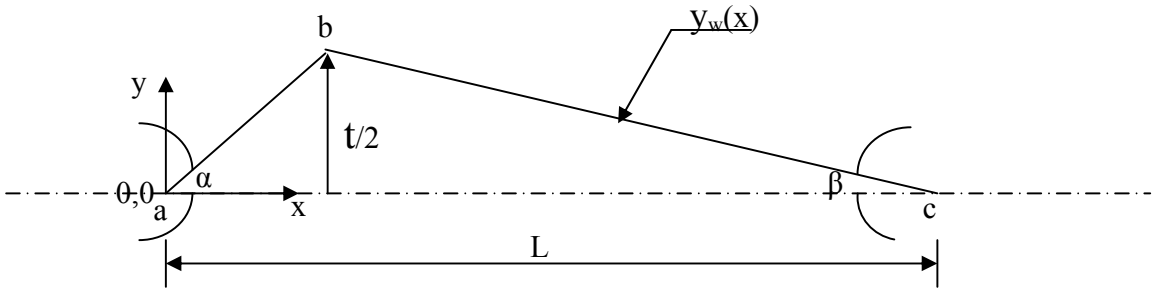

Fig. (1): Problem geometry and coordinate system.

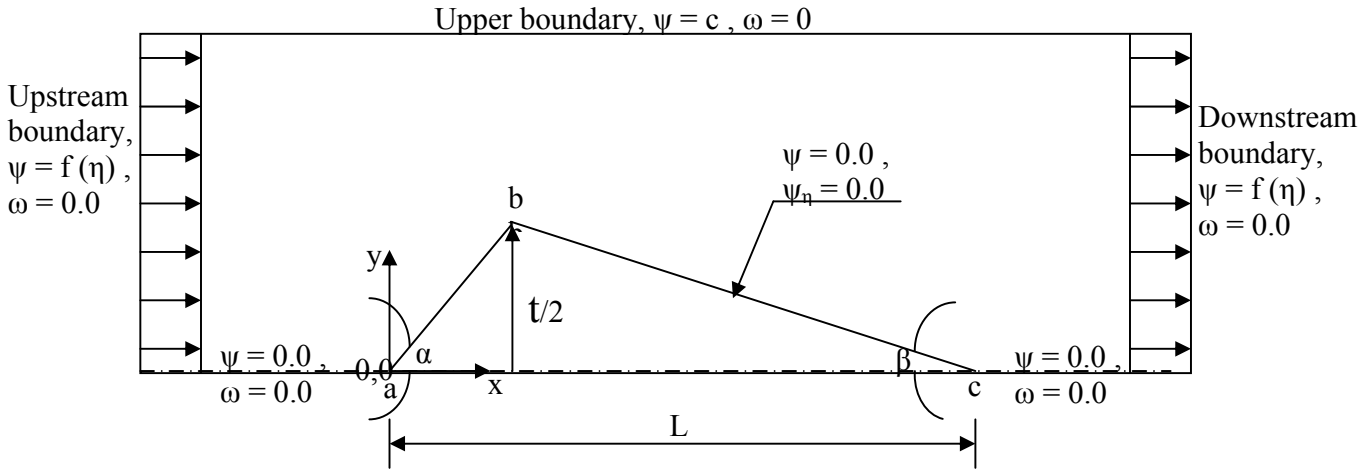

Fig. (2): Solution domain and boundary conditions.

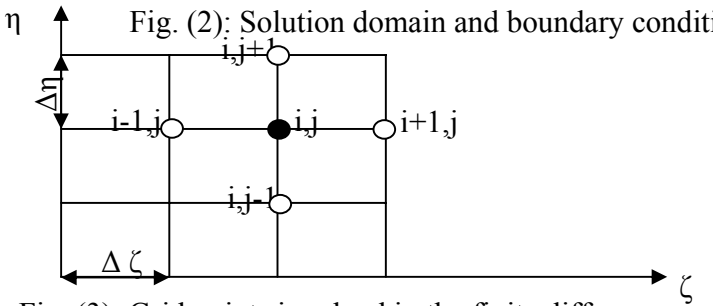

Fig. (3): Grid points involved in the finite difference equations.

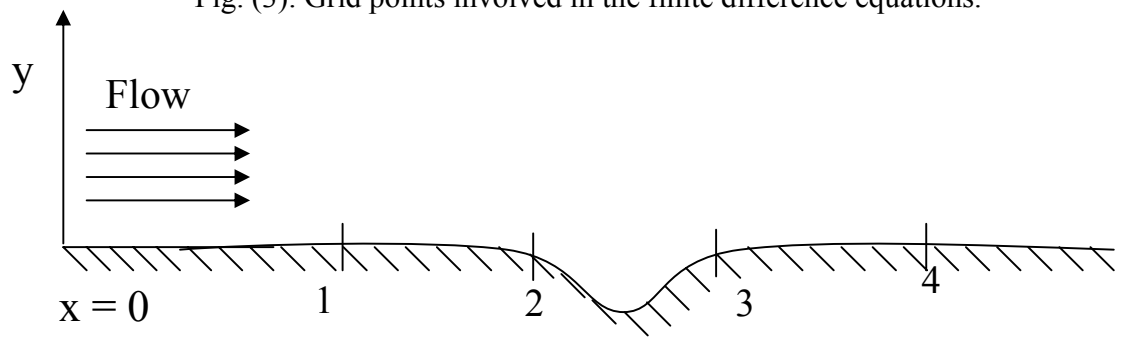

Fig. 4: Dented plate for calculations of separation bubbles, Re = $8x10^4$ [15, 16].

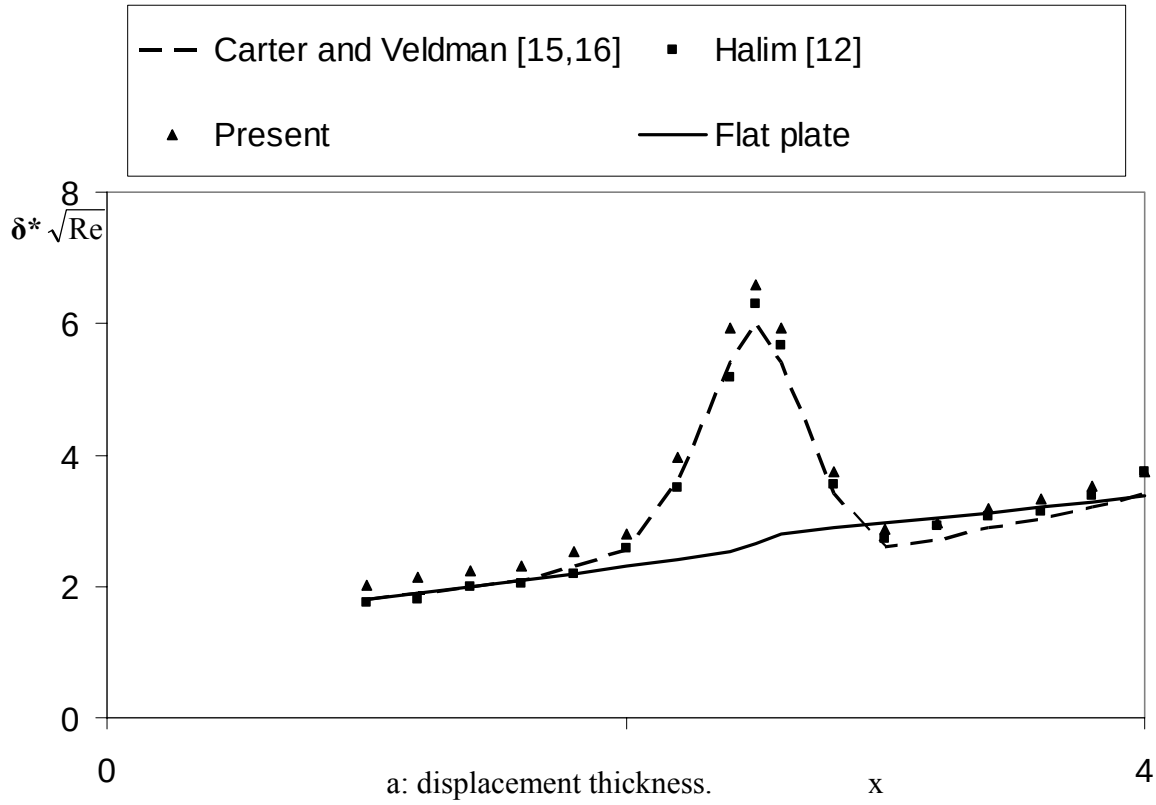

a: displacement thickness.

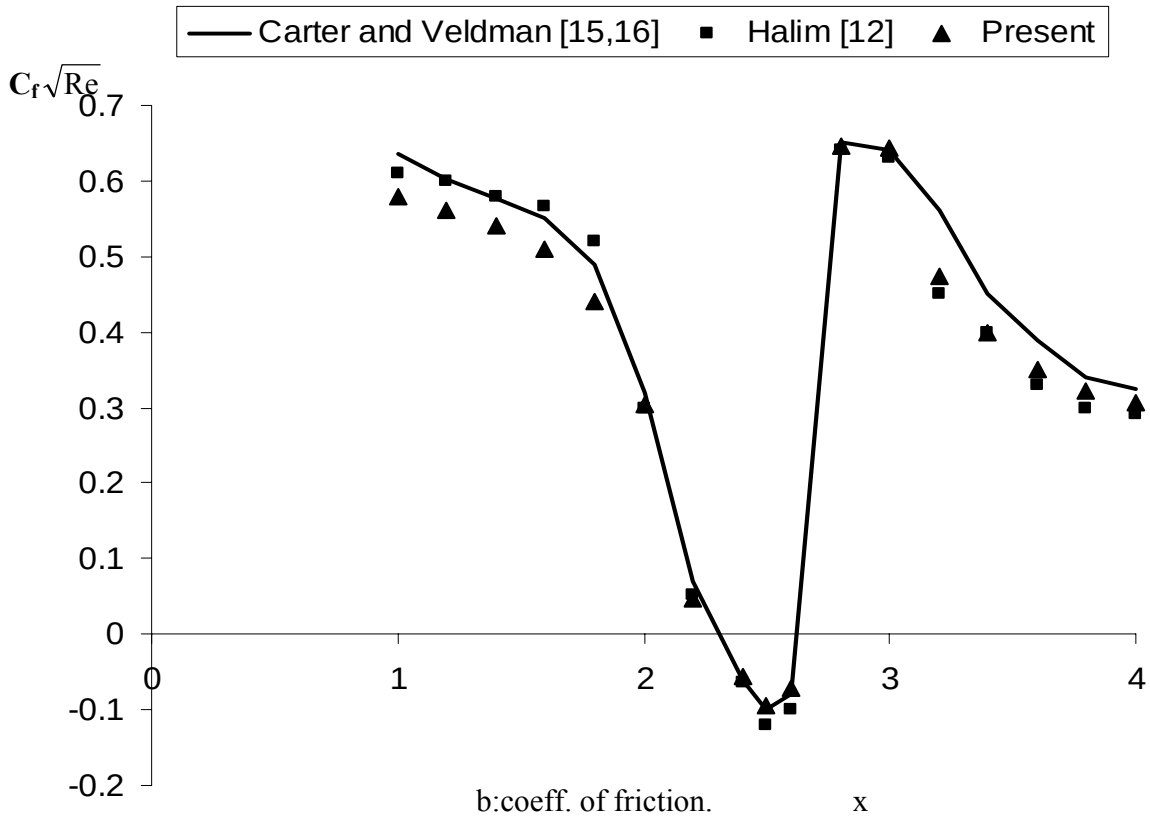

b:coeff. of friction.

Fig. 5: Incompressible laminar separation bubble over a flat plate with a trough. ($Re = 8x10^4$).

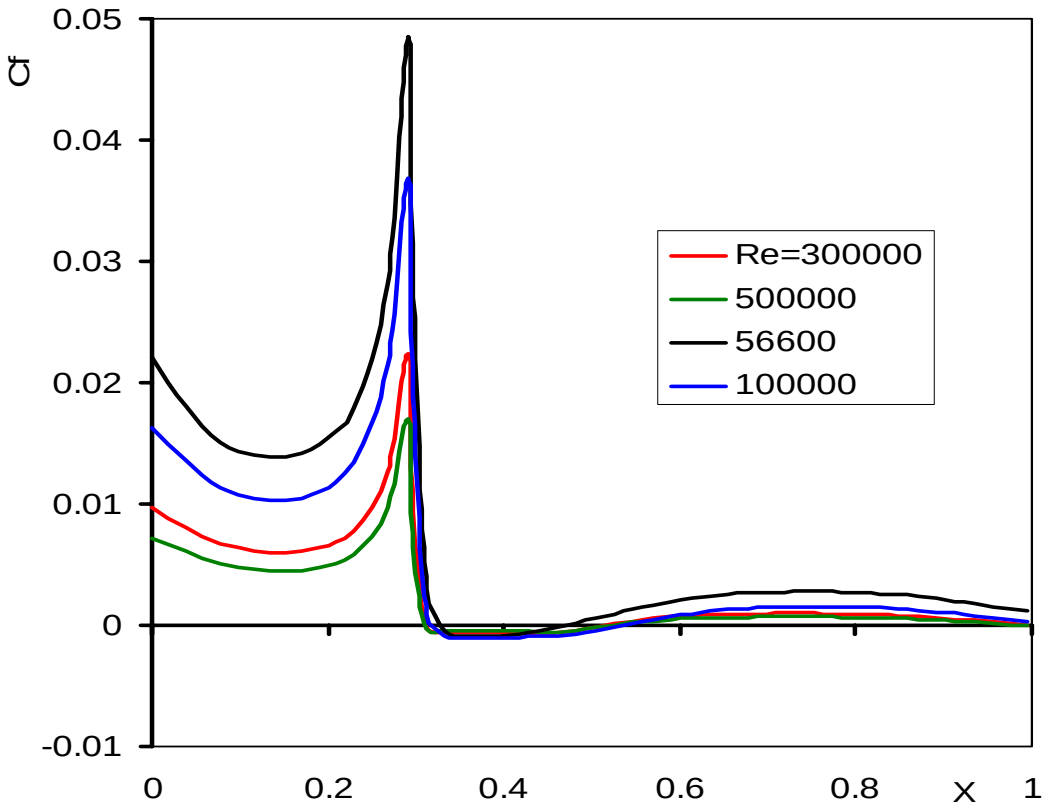

Fig.6a:Wall coefficient of friction (t=0.16 , appex angle=30).

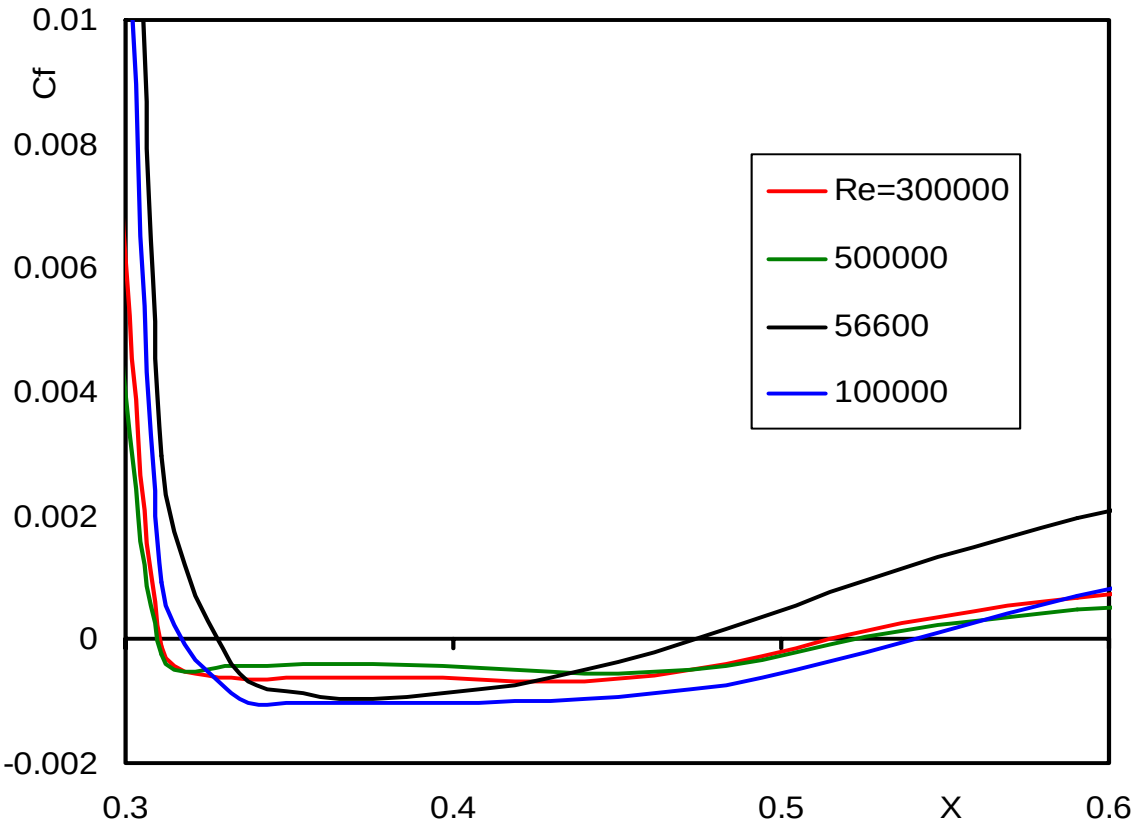

Fig.6b :Bubble wall coefficient of friction.

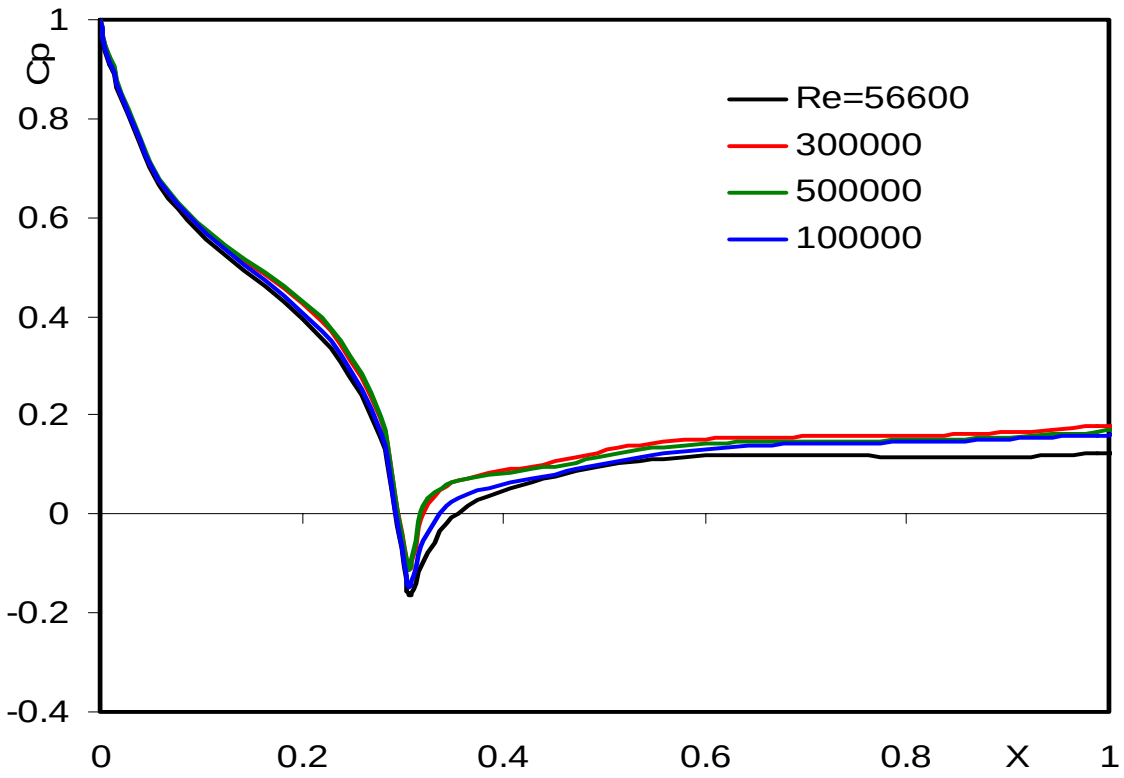

Fig.7a: Coefficient of pressure (t=0.16, leading apex angle=30)

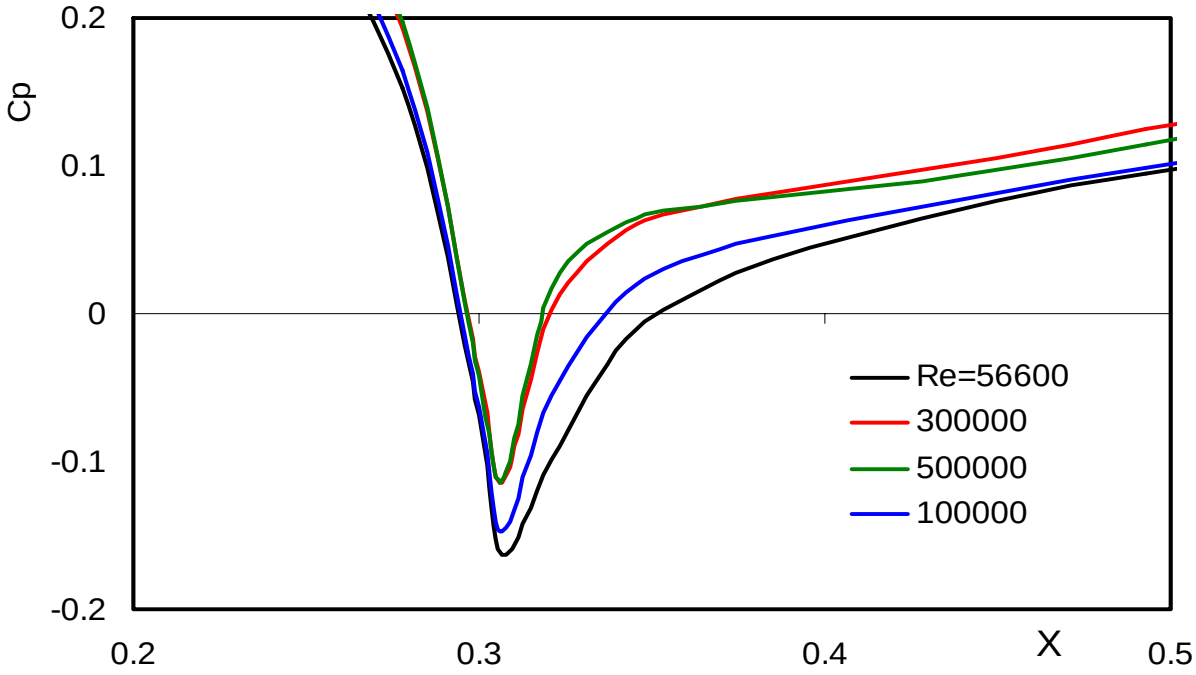

Fig.7b :Coefficient of pressure (t=0.16, leading apex angle=30) .

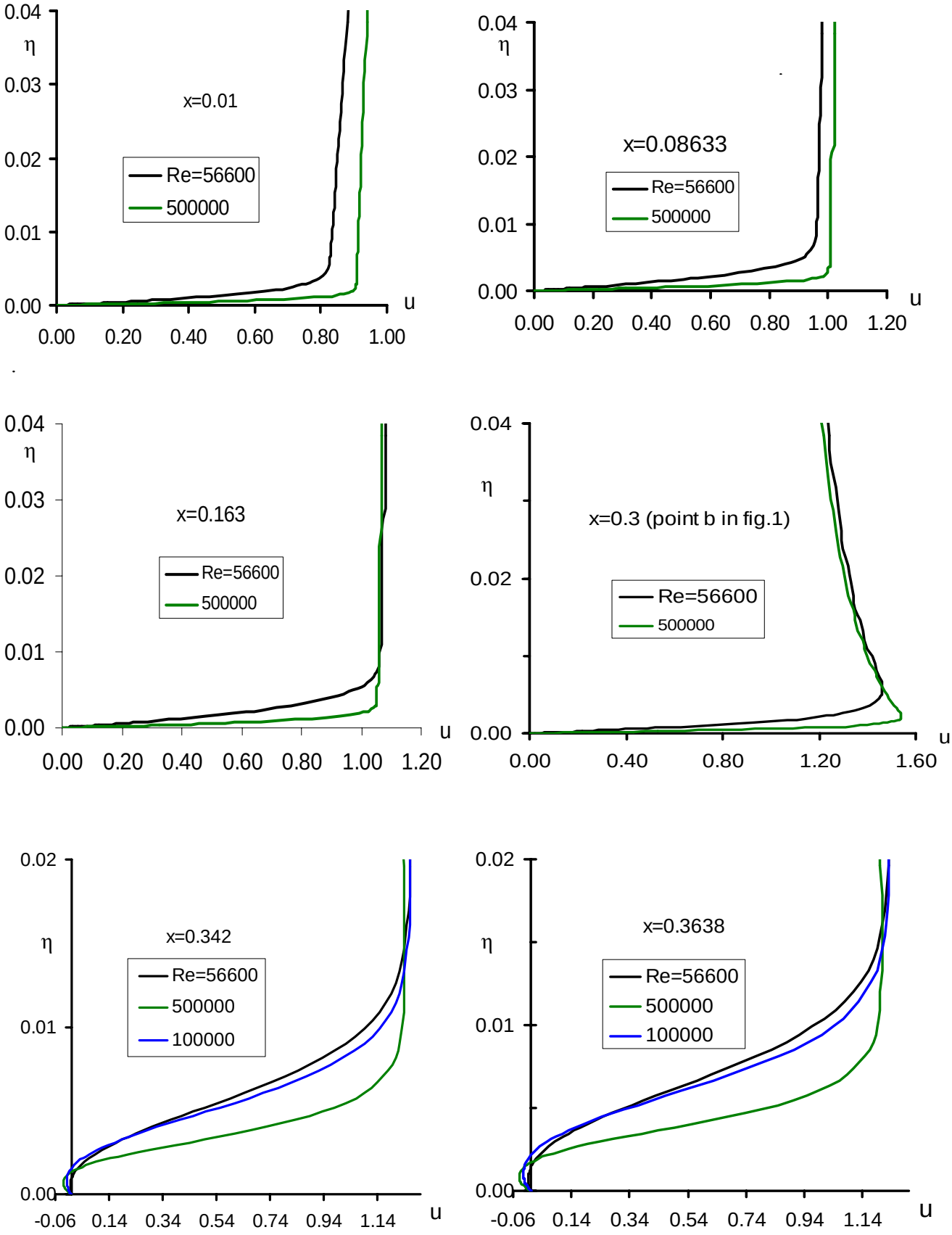

Fig. (8): Development of the streamwise velocity component.

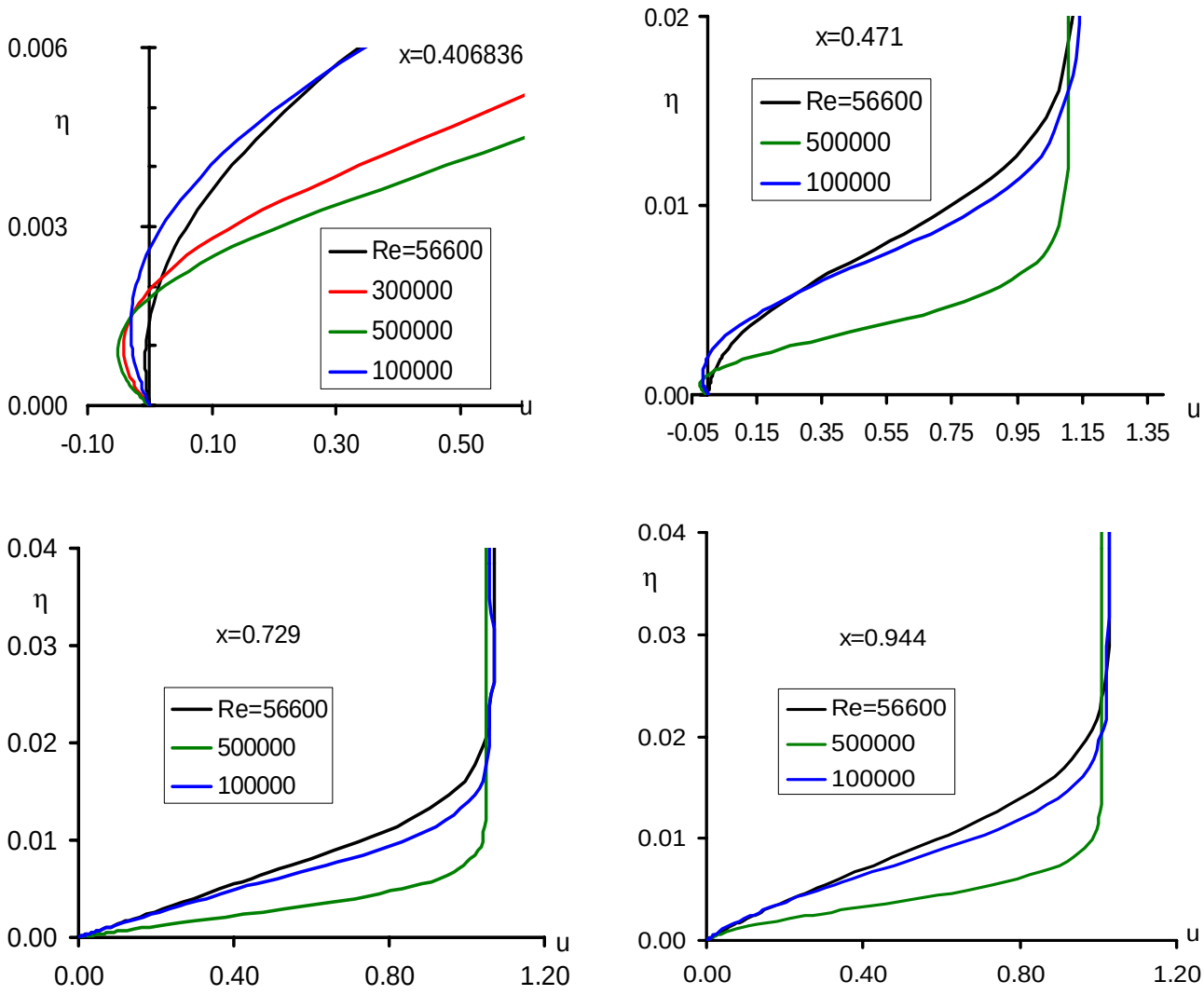

Fig. (8): Continued.

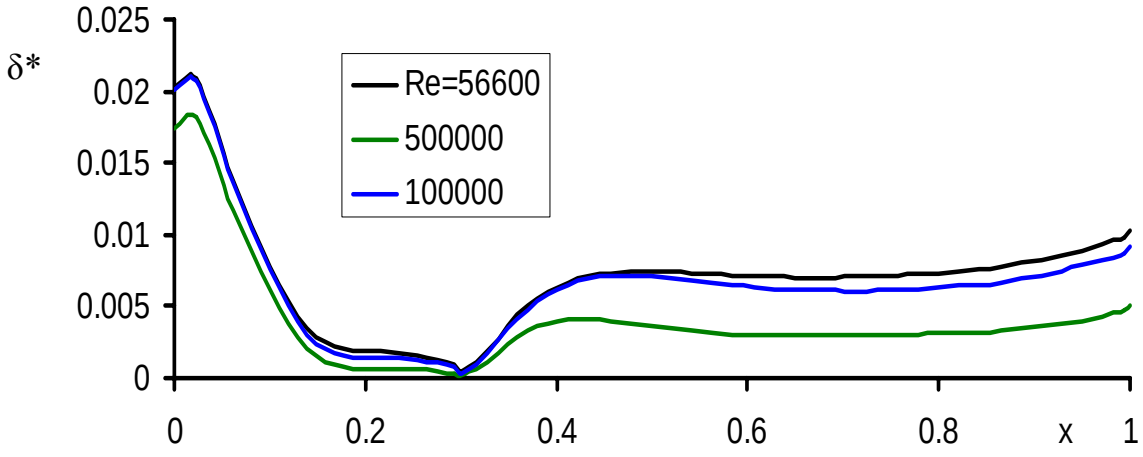

Fig.(9):Displacement Thickness Distribution ·